

Vortex depinning in Josephson-junction arrays

E. K. F. Dang and B. L. Györfy

H. H. Wills Physics Laboratory, University of Bristol, Bristol BS8 1TL, United Kingdom

(Received 23 June 1992; revised manuscript received 19 October 1992)

On the basis of a simple model we study the supercurrent-carrying capacity of a planar array of Josephson junctions. In particular we investigate the zero-temperature vortex-depinning current i_c^B , which is the largest supercurrent in an array containing one extra vortex on top of the ground-state vortex superlattice induced by an external magnetic field f . In the zero-field, $f=0$, case our results support the tilted-sinusoidal vortex-potential description of previous workers. However, in the fully frustrated, $f=\frac{1}{2}$ case, a more careful interpretation is required. We find that on the application of a transport current, the resulting vortex motion is not that of the extra vortex moving over a rigid field-induced vortex background. Rather, a vortex belonging to the checkerboard ground-state pattern first crosses over a junction into a neighboring “empty” plaquette. Then, the “extra” vortex moves to take its place. Our interpretation is based on a linear stability analysis, with the onset of vortex motion being associated with the vanishing of one eigenvalue of the stability matrix. Further applications of the method are suggested.

I. INTRODUCTION

Two-dimensional arrays of Josephson-coupled superconductors have been a subject of considerable experimental¹⁻⁵ and theoretical⁶⁻¹⁵ interest. Technologically as well as scientifically, one of their most significant properties is their supercurrent-carrying capacity. In what follows we shall specifically investigate the largest supercurrent or, equivalently, the critical current for the onset of vortex motion in a square array containing one extra vortex on top of the ground-state vortex superlattice induced by an external magnetic field.^{4,7,8}

The uniform external field, applied perpendicularly to the array, is parametrized by a flux factor f , which is equal to the number of flux quanta threading through each plaquette of the lattice. Extra vortices may be either introduced by small deviations of the flux factor from zero or low-order rationals $f=p/q$ or spontaneously created by thermal fluctuations. Their contribution to the resistive properties of the array is due to their response to a transport current driven through the system. While pinned to some energetically favorable regions of space,^{4,9} vortices do not give rise to a resistive voltage across the sample. But when they begin to move perpendicularly to the current, under the influence of the Lorentz force, a phase slip of 2π occurs at every junction over which a vortex crosses. The associated time-dependent phase difference at the junction implies a voltage drop in the direction of the current. This constitutes a discrete analog of flux-flow resistance which occurs in continuum superconductors. The critical current i_c^B is the current at which the vortices are depinned and hence a finite voltage appears.

Several authors have described the current-induced depinning of individual vortices in terms of a tilted vortex-potential model.^{4,16} Based on this model, Rzchowski

*et al.*⁴ derived an expression for the thermally activated voltage-current characteristic. One important parameter that enters into this expression is the energy barrier E_B that prevents vortex motion. In the zero-field case, the experimental value for E_B of $0.34J$, where J is the Josephson-coupling constant, is about 1.7 times the theoretical prediction.⁴ In the fully frustrated, or $f=\frac{1}{2}$, case, however, the experimental E_B was smaller than the theoretical prediction by a factor of 3. Consequently, it was suggested that in this latter case, at least, a more complex description than the simple vortex potential might be needed.

In this paper we present direct calculations of the zero-temperature vortex-depinning current i_c^B . For $f=0$, our results support the tilted vortex-potential description. For $f=\frac{1}{2}$, however, we find that a more careful interpretation is required. By studying the fluctuation modes of the current-carrying states of the system, we identify the mechanism for vortex motion in this latter case as a two-step process, in which the underlying field-induced vortex background becomes distorted as an “extra” vortex moves along.

For carrying out our calculations, we find it useful to introduce a type of variable that describes stationary states of the Josephson-junction array. We call these variables “loop currents”.¹⁵ They are defined on the dual lattice of the physical array, i.e., on individual plaquettes, as shown in Fig. 1. The corresponding formalism is given in Sec. II. The calculations for $f=0$ and $\frac{1}{2}$ are described and their results presented in Secs. III and IV, respectively. In Sec. V we show that a linear stability analysis of the current-carrying stationary states is a simple but powerful method for identifying the mechanism of vortex depinning, while in Sec. VI we assess the significance of the results and suggest possible further applications of the method.

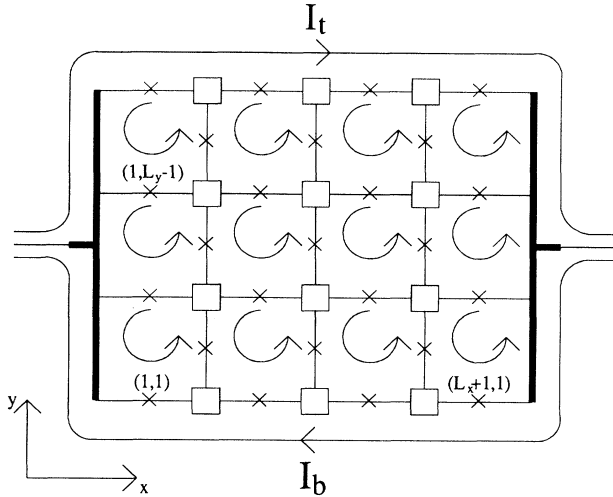


FIG. 1. Loop current representation of a stationary state, shown for a finite array of $L_y \times L_x$ lattice sites. The crosses denote the Josephson junctions between the superconducting islands (represented by small squares). The islands on the left and right edges are coupled to two busbars used to inject a transport current into the array. Also shown are mesh currents I_i and I_b flowing around the outer edges.

II. MODEL AND THE LOOP CURRENT FORMALISM

A much used, simple model for describing weakly coupled arrays of point superconductors is specified by the Hamiltonian

$$\mathcal{H} = -J \sum_{\langle ij \rangle} \cos(\theta_i - \theta_j - A_{ij}), \quad (1)$$

where θ_i is the phase of the complex superconducting order parameter at the site i and $A_{ij} = (2\pi/\Phi_0) \int_i^j \mathbf{A} \cdot d\mathbf{l}$ is proportional to the integral of the vector potential \mathbf{A} from site i to j , with Φ_0 being the flux quantum.⁵⁻¹⁵ The sum in (1) runs over all pairs of weakly coupled superconductors, so that it simply represents the total of all individual Josephson-coupling energies in the array. The Josephson tunneling current between two sites is given by the relation

$$I_{ij} = \frac{2e}{\hbar} J \sin(\theta_i - \theta_j - A_{ij}).$$

In the limit where the magnetic field induced by supercurrents flowing in the array is small compared to the uniform external field \mathbf{H} , the sum of the phase factors A_{ij} around a plaquette is equal to

$$\sum_{ij \in n} A_{ij} = 2\pi \frac{Ha^2}{\Phi_0} = 2\pi f, \quad (2)$$

where the sum is taken in an anticlockwise direction and a is the lattice constant. The sum of the gauge-invariant phase differences $\gamma_{ij} = \theta_i - \theta_j - A_{ij}$ around a plaquette n is then

$$\sum_{ij \in n} \gamma_{ij} = -2\pi f \pmod{2\pi} \\ \gamma = 2\pi(v_n - f). \quad (3)$$

Here v_n is an integer and arises because each of the phases θ_i is defined modulo 2π . For definiteness, we define the *vorticity* of a plaquette n as the value of v_n obtained in (3) when each γ_{ij} in the sum is reduced to lie within the range $[-\pi, \pi]$, as considered by Korshunov and Uimin.¹⁷ In analogy to the Coulomb gas representation^{7,8,18} of the model (1), the variable $q_n = v_n - f$ is termed the “charge” of the plaquette n .

The ground state of the system is the configuration of phases $\{\theta_i\}$ which globally minimize the Hamiltonian (1). This is one of the stationary points of \mathcal{H} . Monte Carlo calculations^{7,8,10} have shown that, at rational fields $f = p/q$, the lowest-energy state is spatially periodic, with a $q \times q$ unit cell, in which vortices, or equivalently charges, are arranged in a regular superlattice. In particular, Halsey¹⁰ proposed that in the range $\frac{1}{3} \leq f \leq \frac{1}{2}$ with small q the ground states are characterized by constant phase differences along diagonal “staircases,” which consist of alternating vertical and horizontal junctions. These correspond to diagonal lines of positive $(1-f)$ charges separated by line(s) of negative $(-f)$ charges, with the total charge in each unit cell summing to zero. Alternatively speaking, such states consist of diagonal lines of unit and zero vorticities. Vortex excitations of the Kosterlitz-Thouless type⁸ result from adding “extra vortices” Δv_n on top of the ground-state vortex pattern $\{v_n^0\}$:

$$v_n = v_n^0 + \Delta v_n, \quad (4)$$

where Δv_n , like v_n^0 , is an integer.

To study zero-temperature properties, we minimize the Hamiltonian (1) with respect to the independent variables $\{\theta_i\}$. The Euler-Lagrange equation for this problem is

$$J \sum_j \sin(\theta_i - \theta_j - A_{ij}) = 0 \quad \text{for all } i, \quad (5)$$

which is recognized as Kirchhoff’s law of current conservation applied at the lattice sites i . Consequently, stationary states of the Hamiltonian (1) can be represented by systems of “loop currents” $\{I_n\}$ flowing around in every plaquette (Fig. 1). We define the positive sense of the loop currents as anticlockwise. They are thus related to the phase differences on the junctions through

$$\sin \gamma_{ij} = I_{(ij,L)} - I_{(ij,R)}, \quad (6)$$

where the two terms on the right-hand side denote the loop currents (in units of the single-junction critical current $i_{c0} = 2eJ/\hbar$) to the left and right of the link ij .

It should be noted that not every arbitrary set of loop currents $\{I_n\}$ constitutes a stationary state of the model—for example, Eq. (6) shows that the difference between the two loop currents on neighboring plaquettes must not be greater than unity in magnitude. More specifically, for a fixed magnetic field f , since the sum of phase differences around each plaquette must satisfy the “quantization relation” [Eq. (3)], we arrive at the following constraint on the loop currents:

$$\sum_m \arcsin(I_n - I_m) = 2\pi(v_n - f), \quad (7)$$

where the sum is over plaquettes neighboring to n . The range of the arcsin function is restricted to $[-\pi, \pi]$.

The form of Eq. (7) makes it natural to solve for stationary states $\{I_n\}$ that correspond to specific vorticity configurations $\{v_n\}$. For a given $\{v_n\}$, Eq. (7) must be combined with appropriate boundary conditions in order to yield unique solutions. We are primarily interested in those boundary conditions that impose a desired net transport current across the array. Two of such conditions have been investigated.

The first of these, called twisted periodic conditions, are useful for simulating an infinite periodic system. For a system with a $L_y \times L_x$ unit cell, these conditions are given by

$$\begin{aligned} I(x + L_x, y) &= I(x, y) - L_x I_v, \\ I(x, y + L_y) &= I(x, y) + L_y I_h, \end{aligned} \quad (8)$$

where I_v and I_h are, respectively, the average vertical and horizontal components of the transport current per junction. It can be seen from Eq. (7) that the boundary conditions (8) will determine the loop currents only up to an additive constant. We therefore impose an additional arbitrary condition

$$\sum_{\text{unit cell}} I(x, y) = 0, \quad (9)$$

which effectively serves to fix this constant. Applications of these conditions in determining the intrinsic critical current I_{c0} , which is the largest supercurrent for which a metastable state exists, have been presented elsewhere.¹⁵

The second of the boundary conditions apply to a finite lattice of $L_y \times L_x$ sites, with a geometry that has been studied by Rzchowski *et al.*⁴ The superconductors on the left and right edges are coupled to two vertical busbars used to inject a horizontal transport current into the array (Fig. 1). As shown in Fig. 1, in addition to the loop currents flowing within the array, there are mesh currents I_t and I_b that flow around the outer edges. To impose a net current of I_h per horizontal junction, I_t and I_b are fixed such that

$$I_t = -I_b = L_y I_h / 2. \quad (10)$$

These may equivalently be represented by two fictitious rows of loop currents at the top and bottom of the real array:

$$\begin{aligned} I(x, L_y) &= +L_y I_h / 2, \\ I(x, 0) &= -L_y I_h / 2. \end{aligned} \quad (11)$$

For a fixed vorticity configuration $\{v_n\}$, Eq. (7) together with the appropriate boundary conditions can be solved with a multidimensional Newton-Raphson method.¹⁹ More specifically, corrections to an initial estimate $\{I_n^0\}$ of the solution are obtained by solving the following coupled set of linear equations:

$$\sum_l \frac{\partial f_k}{\partial I_l} \delta I_l^0 = -f_k(\{I_n^0\}), \quad (12)$$

where

$$f_{k(x,y)} = 2\pi[v_{k(x,y)} - f] - \sum_l \arcsin[I_{k(x,y)} - I_{l(x',y')}], \quad (13)$$

in which the sums are over neighboring plaquettes to k . The process is repeated iteratively until convergence is reached. It turns out that the iteration can be stabilized if a fraction Δ_M , called the ‘‘mixing factor,’’ of the correction δI_n^0 , rather than the full value, is added to the old estimate at each step. This is similar to the ‘‘under-relaxation’’ method of Cohn *et al.*²⁰ Values of Δ_M between 0.3 and 0.6 are found to be satisfactory. Since each loop current is only coupled to those belonging to neighboring plaquettes, the matrix representing the linear equation (12) is extremely sparse. In fact, for a $L \times L$ lattice, the number of nonzero elements in the matrix is proportional to L^2 , compared to the total number of elements being L^4 . We have simulated lattices of up to 64×64 plaquettes.

III. CURRENT-INDUCED VORTEX-DEPINNING IN THE ZERO-FIELD CASE

We first consider a single extra vortex on a finite array in zero magnetic field and with zero net transport current. In this case, $A_{ij} = 0$ on all junctions. Then the ground state, with all phases θ_i aligned, obviously corresponds to $v_n^0 = 0$ on all plaquettes. The single-vortex state is given by $\Delta v_v = +1$, where v denotes the plaquette in which the vortex ‘‘center’’ is located. Figures 2(a)–2(c) show three equivalent representations of such a state in a 12×12 array. In Fig. 2(a) the angle of the arrows measured from the y axis denotes the phase of the superconducting order parameters θ_i . Figure 2(b) displays the direction and magnitude of supercurrents flowing on every junction. In Fig. 2(c) the magnitudes of the loop currents on all the plaquettes are presented as a three-dimensional plot. Since the loop currents are defined on the discrete dual lattice of the physical array, the lines drawn in Fig. 2(c) are only a guide to the eye. Nonetheless, for a large lattice, the loop currents for $f = 0$ vary smoothly with distance away from the vortex center. One can easily obtain the functional form of the loop currents in the continuum limit as $I(r) \propto -\ln(r/a)$ for large r and away from the edges, where r is the distance from the vortex center. This corresponds to supercurrents circulating around the vortex center that fall off as $1/r$ [Fig. 2(b)].

In order to check the effect of edges in the finite system, we have investigated the size dependence of the single vortex energy for the fields $f = 0$, $\frac{1}{2}$, and $\frac{1}{3}$ (Fig. 3). Figure 3 shows that the expected logarithmic dependence^{4,21} is observed right down to the smallest system studied, thus indicating that the edge effect is not important.

Lobb, Abraham, and Tinkham⁹ have shown that at $f = 0$ there are two possible single-vortex stationary states, with one being an energy minimum and the other an energy maximum. The solution presented in Figs. 2(a)–2(c), with the vortex center coinciding with the center of a plaquette, corresponds to the energy

minimum. The energy maximum corresponds to the other solution for which the vortex center is positioned on top of a junction, midway between two plaquettes. Vortex motion out of one low-energy position into an equivalent site one lattice constant away is therefore prevented by an energy barrier E_B , which was calculated to be $0.199J$ in the limit of large lattice sizes. Rzechowski *et al.*⁴ subsequently extended this picture to yield a complete two-dimensional energy surface that represents a "vortex-pinning potential" in the array. This potential was shown to be very close to a pure sinusoid.⁴

When a transport current flows in a type-II supercon-

ductor, a magnetic-flux (or vortex) line experiences a Lorentz force given by

$$\mathbf{f} = \mathbf{J} \times \Phi_0 / c, \quad (14)$$

where \mathbf{J} is the current density. One might expect that in the Josephson-junction array, a transport current will have an analogous effect on a vortex. This is generally described as a tilting of the sinusoidal vortex potential transversely to the direction of current flow.^{4,16} The zero-temperature critical current for the onset of vortex motion, i_c^B , is reached when the Lorentz force equals the

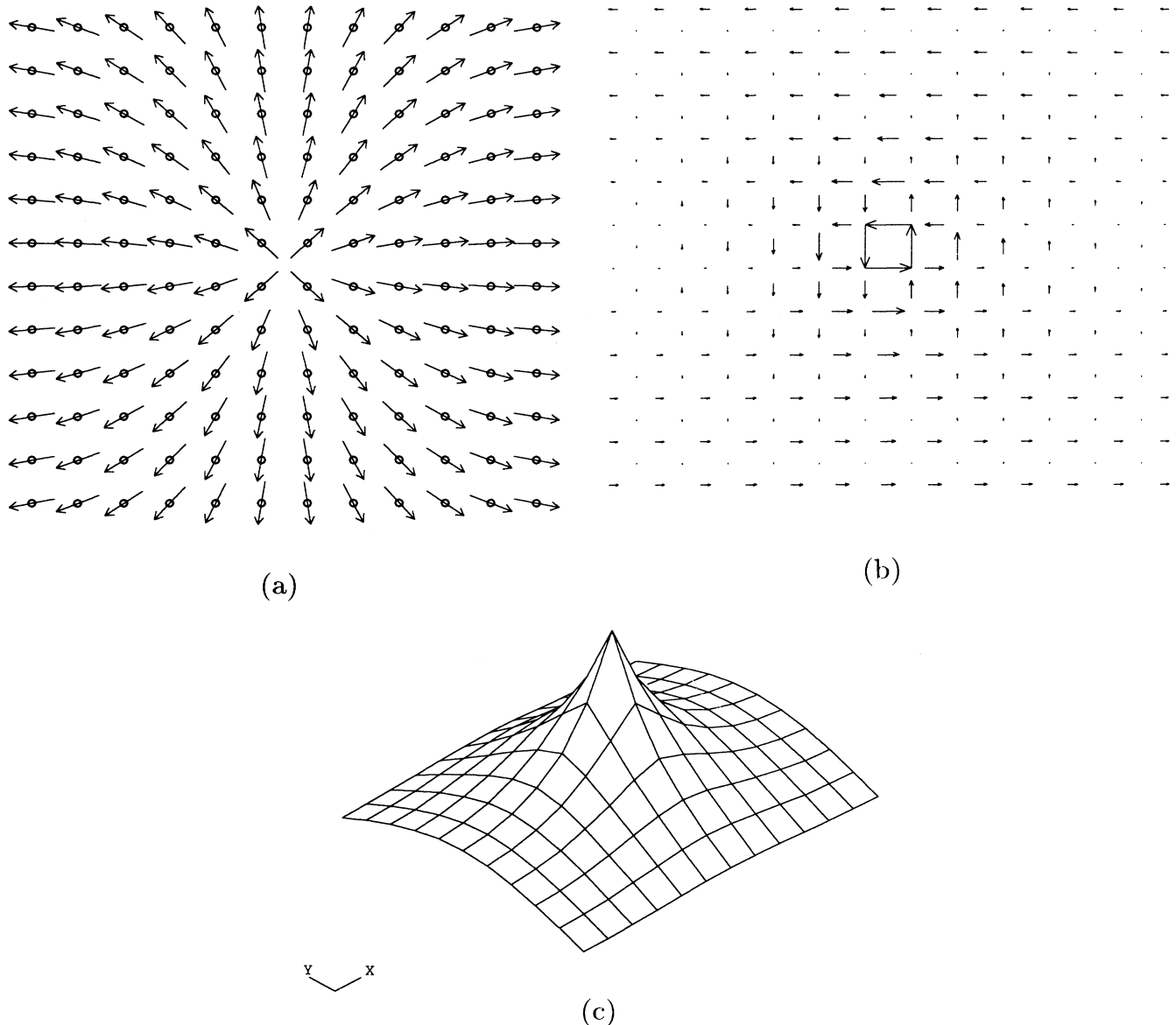


FIG. 2. Three equivalent representations of a single-vortex state for $f=0$, on a 12×12 lattice. The array is coupled to two bus-bars (not shown) on the left and right edges. (a) and (b) are after Rzechowski *et al.* (Ref.4). In (a) are shown the phases of the superconducting order parameters, in (b) the Josephson currents flowing between lattice sites, and in (c) the magnitude of loop currents on each plaquette, the cusp corresponding to the vortex center.

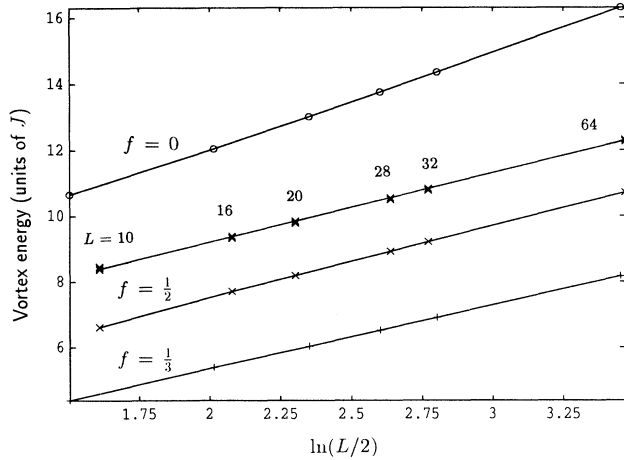


FIG. 3. Size dependence of the single-vortex energy for $f=0$ (\circ), $\frac{1}{2}$ (\times), and $\frac{1}{3}$ ($+$). L is the number of plaquettes along each side of a square array. For $f=\frac{1}{2}$, the low- and high-energy lines shown in the figure correspond to $q_v = +\frac{1}{2}$ and $+\frac{3}{2}$, respectively.

maximum restoring force of the pinning potential. From (14) one obtains $i_c^B = eE_B/\hbar$ for a sinusoidal potential, and so $i_c^B \sim 0.1i_{c0}$.⁴ Although this scenario is quite plausible, it is not immediately obvious how the Lorentz force arises in the present simple model, especially when the magnetic effects of the circulating supercurrents have been neglected. Nonetheless, in what follows we will demonstrate that our numerical results are consistent with the tilted vortex-potential description and from them deduce i_c^B .

Using the finite array boundary conditions (10), we seek single-vortex states that carry a net horizontal transport current. By starting at appropriate initial estimates of the loop current configurations $\{I_n^0\}$ [Eq. (12)], we find two solutions at each current. Their energy-current relations are shown in Figs. 4(a) and 4(b) for the 6×6 and 12×12 lattices, respectively. In particular, the two solutions at zero current, $I_h=0$, correspond to the energy minimum and maximum obtained by Lobb, Abraham, and Tinkham.⁹ The figures show that at small currents both the low- and high-energy branches rise parabolically. However, they merge at some critical value of current, above which no solution exists.

According to Eq. (14), we anticipate that a net horizontal current will exert a force on a vortex in the vertical direction (i.e., along the y axis). The associated “tilting” of the sinusoidal vortex potential may then be described analytically by adding to it a component that varies linearly with y . This results in a deviation of the energy minima and maxima from their zero-current positions, such that they move toward each other in pairs. Eventually, when the current reaches a critical value, the minima and maxima merge, becoming points of inflection and thus reducing the energy barrier to zero. At higher currents, no stationary point exists. Therefore we identify the maximum supercurrent for which a metastable

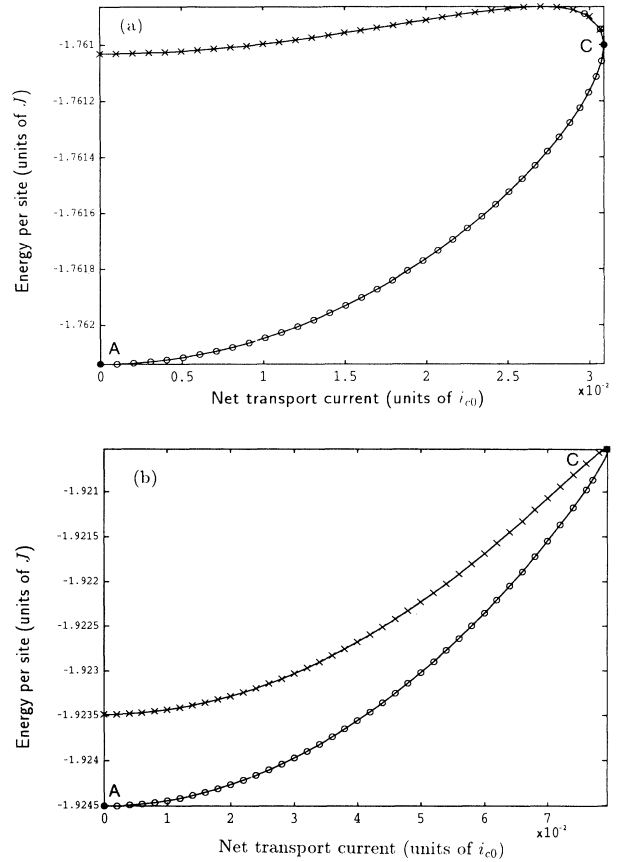


FIG. 4. Energy per site vs net current for $f=0$ single-vortex states on a (a) 6×6 and (b) 12×12 lattice.

state exists as the vortex-depinning current i_c^B . As shown in Fig. 5, in the limit of large lattice sizes, $i_c^B(f=0)$ extrapolates to $\sim 0.102i_{c0}$, in agreement with the rough approximation as presented above and the numerical result of Rzchowski *et al.*⁴

The main reason why we have used finite, rather than periodic boundary conditions here is as follows. For a

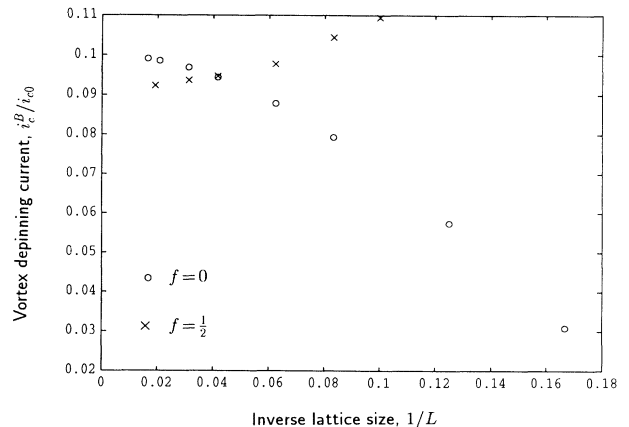


FIG. 5. Vortex-depinning current i_c^B/i_{c0} as a function of the inverse lattice size, for $f=0$ (\circ) and $f=\frac{1}{2}$ (\times).

periodic system, summing both sides of Eq. (3) over a unit cell readily shows that the total charge in the unit cell must be zero, because each γ_{ij} will be summed over twice, but in opposite senses. Therefore, with periodic boundary conditions, a vortex-antivortex pair needs to be introduced, instead of the desired single extra vortex.

IV. VORTEX DEPINNING IN THE FULLY FRUSTRATED CASE

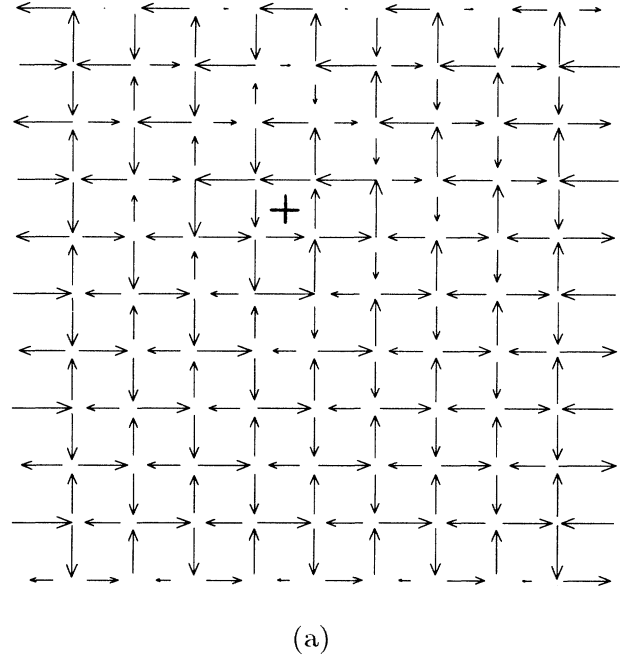
At $f = \frac{1}{2}$, for which the ground state corresponds to a checkerboard arrangement of unit and zero vortices,^{8,10} there are two distinct positions where an extra vortex ($\Delta v = +1$) may be added. This can be either at a plaquette with an original charge of $q = -\frac{1}{2}$ (i.e., $v^0 = 0$) or at one with $q = +\frac{1}{2}$ (i.e., $v^0 = 1$). These will lead to new values of the charge of $q_v = +\frac{1}{2}$ or $+\frac{3}{2}$, respectively, where v denotes the plaquette to which the extra vortex is added.

For both cases, we solved the loop current equation (7) iteratively by starting at a large number of random initial configurations $\{I_n^0\}$. For $q_v = +\frac{1}{2}$, only one solution is found at small currents. However, for $q_v = +\frac{3}{2}$, we found a large number of solutions. Figures 6(a) and 6(b), respectively, display the $q_v = +\frac{1}{2}$ state and one of the $q_v = +\frac{3}{2}$ states at zero net current. The nature of the $q_v = +\frac{3}{2}$ states may be understood as follows. For this vortex pattern, Eq. (3) shows that the sum of the gauge-invariant phase differences around the plaquette v is $\sum \gamma = 2\pi q_v = 3\pi$. The different solutions correspond to different ways in which this sum may be divided among the four junctions. Neglecting finite-size effects, the state shown in Fig. 6(b), for example, corresponds to a symmetric distribution such that each phase difference around v is equal to $3\pi/4$. The other solutions correspond to various asymmetric divisions of the total sum.

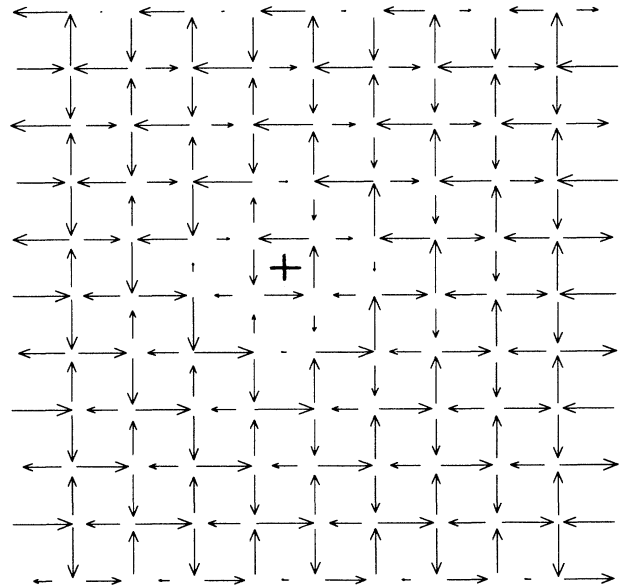
In the work of Rzchowski *et al.*,⁴ it was assumed that under the influence of a transport current Lorentz force the extra vortex would move over the array without distorting the underlying checkerboard vortex background. Therefore, for a vortex to move from a plaquette with zero background vorticity ($v^0 = 0$) to an equivalent position two lattice constants away, it must pass over a plaquette with $v^0 = +1$. In other words, it must go from a $q_v = +\frac{1}{2}$ state to a $q_v = +\frac{3}{2}$ state. It was found that the $q_v = \frac{3}{2}$ state is higher in energy than the $q_v = \frac{1}{2}$ state by $\Delta E = 1.28J$. The above vortex motion would thus be prevented by a barrier of this height. However, Rzchowski *et al.* derived from the experimental measurements a barrier of only $0.44J$, much lower than the expected value. It was thus clear that a different model for vortex motion should be involved. This is what we seek to identify in the remaining of this paper.

As in the case of $f = 0$, we solved for current-carrying single-vortex states in $f = \frac{1}{2}$, both for $q_v = +\frac{1}{2}$ and $+\frac{3}{2}$. The energy-current relations for the solutions obtained on a 11×9 lattice are plotted in Fig. 7. At the maximum current for which a $q_v = +\frac{1}{2}$ state exists ($0.109i_{c0}$ on the 11×9 lattice), the energy difference between the $q_v = +\frac{1}{2}$

state and any of the $q_v = +\frac{3}{2}$ states is far from zero. Thus, if this maximum current can be interpreted as the vortex-depinning current i_c^B , just as in the $f = 0$ case, then we have immediately disproved the picture of vortex motion over a rigid ground-state superlattice. In the next section, we will demonstrate that the maximum current is



(a)



(b)

FIG. 6. Josephson currents for $f = \frac{1}{2}$ single-extra-vortex states on a 11×9 lattice. (a) shows the $q_v = +\frac{1}{2}$ state, while (b) is the "symmetric" $q_v = +\frac{3}{2}$ state. The + sign denotes an extra unit vorticity ($\Delta v = +1$).

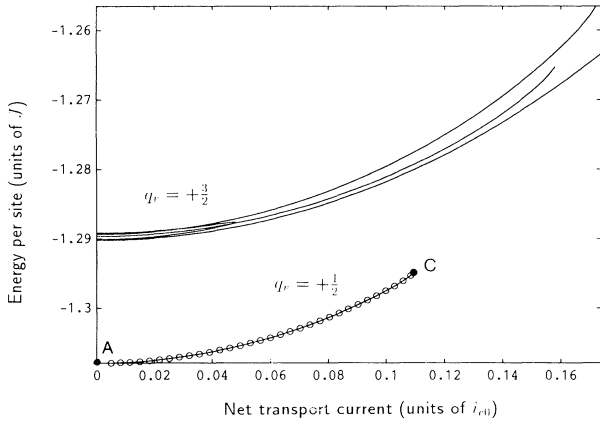


FIG. 7. Energy-current relation for $f = \frac{1}{2}$ single-extra-vortex states on a 11×9 lattice. The circled curve corresponds to $q_v = \frac{1}{2}$, while the plain curves are the $q_v = +\frac{3}{2}$ states.

indeed i_c^B . In our calculations, i_c^B for $f = \frac{1}{2}$ actually decreases with increasing lattice size (Fig. 5), and in the infinite lattice limit, we obtain $i_c^B(f = \frac{1}{2}) \sim (0.092 \pm 0.002)i_{c0}$.

V. STABILITY OF CURRENT-CARRYING STATES

In this section we will describe a systematic method for finding the critical current for vortex depinning and at the same time identifying the way in which vortex motion takes place. The method is based on studying small angle fluctuations $\{\delta\theta_i\}$ about the current-carrying stationary states which are solutions of the Euler-Lagrange equation (5) or, equivalently, the loop current equation (7). More specifically, we carry out a linear stability analysis of these stationary states^{10,13–15} and associate the critical current with the onset of instability. This involves finding the eigenvalues of the stability or Hessian matrix \underline{M} , which has elements

$$M_{ij} = \left. \frac{\partial^2 \mathcal{H}}{\partial \theta_i \partial \theta_j} \right|_{\{\theta_i^0\}}, \quad (15)$$

where $\{\theta_i^0\}$ is the configuration of the stationary state whose stability is being investigated. From the Hamiltonian (1), we find that the diagonal elements are

$$M_{ii} = J \sum_k \cos(\theta_i - \theta_k - A_{ik}), \quad (16)$$

where the sum is over sites coupled to i . For $i \neq j$ the off-diagonal elements are

$$M_{ij} = \begin{cases} -J \cos(\theta_i - \theta_j - A_{ij}) & \text{for nearest neighbors,} \\ 0 & \text{otherwise.} \end{cases} \quad (17)$$

Equation (16) means that the diagonal element M_{ii} is the minus of the sum of the energies of all bonds connected to the site i . The off-diagonal term M_{ij} given in Eq. (17) is the energy of the bond ij if i and j are nearest neighbors and zero otherwise. The “site” indices i should include

the two busbars for the finite lattice considered.

Benedict¹⁴ and Dang, Halász, and Györfy¹⁵ studied the above problem for an infinite periodic system. Using the Bloch’s theorem, they were able to calculate the eigenvalues of the Hessian matrix analytically in some cases. In the present case of a finite, nonperiodic system, however, the eigenvalues must be obtained numerically. Since the Hessian is a very sparse matrix and is symmetric, this is not too difficult a task.

For every stationary state, the Hessian has at least one zero eigenvalue which is associated with the invariance of the Hamiltonian under global phase rotation. A stationary state is metastable, i.e., a local minimum, if all eigenvalues are non-negative. When a negative eigenvalue appears as a result of an increase of the current driven through the system, the state becomes unstable to distortions of the phase pattern $\{\delta\theta_i\}$, specified by the corresponding eigenvector or fluctuation mode. Generally, to study the onset of instability, only a few eigenvalues closest to zero need to be considered.

Figure 8 shows the variation of the lowest eigenvalues above zero for single-vortex states of $f = 0$ (on a 12×12 lattice) and $f = \frac{1}{2}$ (on a 11×9 lattice) as the net current is increased. These correspond to the curves labeled AC in Figs. 4(b) and 7. In both cases, at low currents, all the eigenvalues are positive. At precisely the point C, where the maximum current is reached, there is an abrupt drop in some of the eigenvalues, resulting in one of them becoming zero. This confirms the onset of instability at the maximum currents found previously.

We can interpret the fluctuation modes in terms of the change in the vorticity of individual plaquettes that results from the phase distortions. Suppose the μ th mode is given by $\{\delta\theta_i^\mu\}$; then, a fluctuation with amplitude α_μ will produce a distorted phase pattern of

$$\theta_i' = \theta_i^0 + \alpha_\mu (\delta\theta_i^\mu). \quad (18)$$

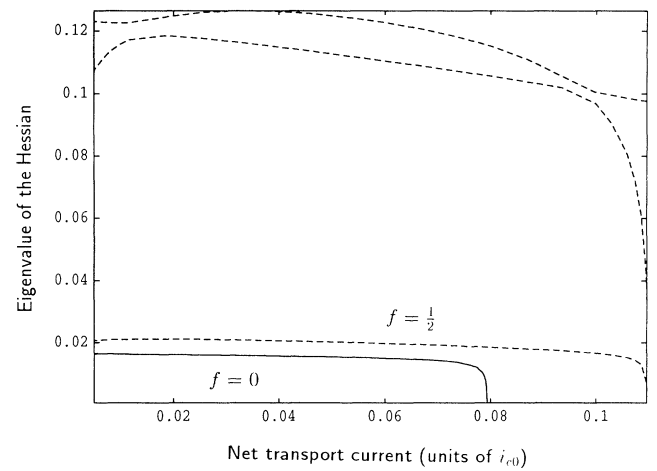


FIG. 8. Variation of the lowest eigenvalues of the stability matrix with the net current. The solid curve is the lowest eigenvalue above zero, for the $f = 0$ single-vortex state on a 12×12 lattice. The dashed curves are the three lowest eigenvalues above zero for the $q_v = +\frac{1}{2}$ state of $f = \frac{1}{2}$, on a 11×9 lattice.

The resulting gauge-invariant phase differences will be

$$\gamma'_{ij} = \theta'_i - \theta'_j - A_{ij}. \quad (19)$$

Now, if each phase difference is restricted to lie in the range $[-\pi, \pi]$, there will be a phase slip of 2π at a junction if the fluctuation causes the phase difference in (19)

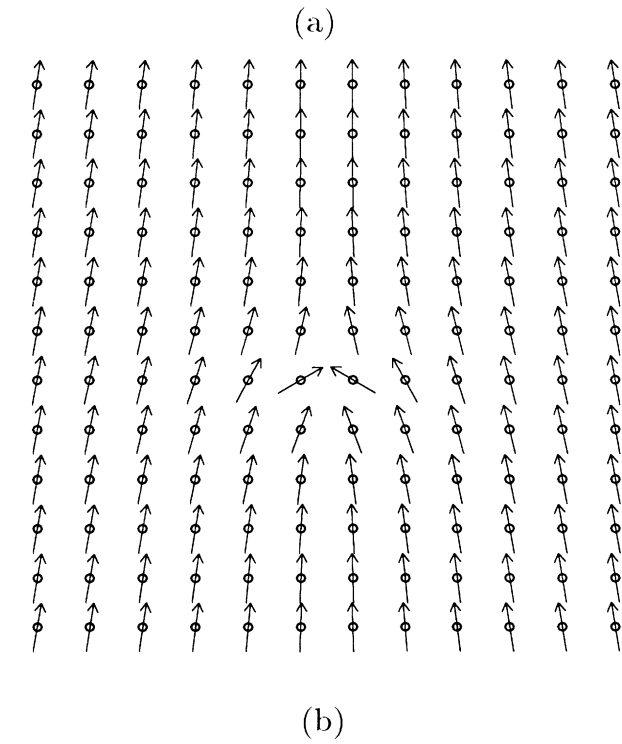
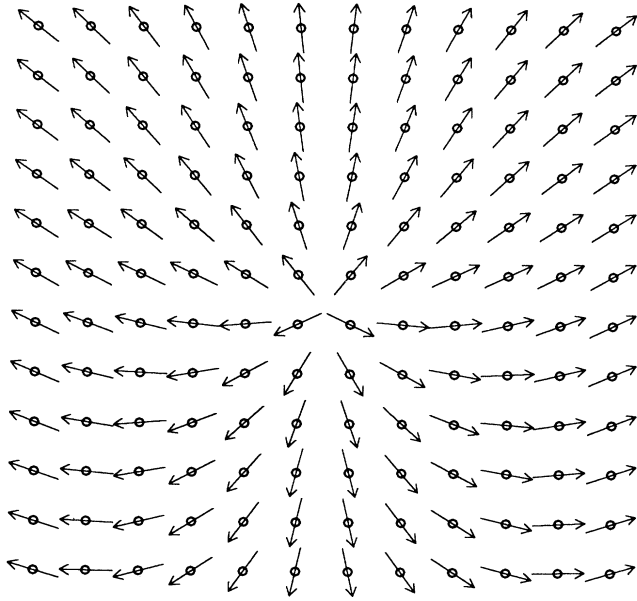


FIG. 9. (a) Unstable $f=0$ single-vortex state (on a 12×12 lattice) at $i_c^B \sim 0.0793i_{c0}$. (b) The fluctuation mode responsible for the instability at i_c^B .

to step out of this range. This will result in a unit increase in the vorticity in one of the two plaquettes bordering the junction and a corresponding decrease for the other one. In other words, a vortex has moved over the junction.

The unstable phase configuration for the $f=0$ single-vortex state at i_c^B [i.e., point C in Fig. 4(b)] is shown in Fig. 9(a). Figure 9(b) displays the eigenvector responsible for the instability. The figure shows large fluctuations near the vortex center. Individual vorticities are calculated according to Eqs. (3), (18), and (19), at increasing amplitudes α_μ of the fluctuation. It is found that when the amplitude reaches ~ 1.43 , phase slip occurs on the “bottom” junction bordering the vortex center, such that the single vortex is moved one plaquette downward.

For $f = \frac{1}{2}$, the fluctuation that causes the instability of the state C is shown in Fig. 10. The similarity between Figs. 9(b) and 10 suggests that in the $f = \frac{1}{2}$ case the fluctuation again corresponds to the movement of a vortex. In this case, however, at a fluctuation amplitude of ~ 1.06 , the phase slip occurs on the bottom junction of the plaquette *below* the extra vortex. This means that the actual vortex that moves is not the “extra” vortex, but one that belongs to the checkerboard superlattice, as shown in Fig. 11(a).

In the light of this result, we investigated stationary states corresponding to the distorted vortex superlattice

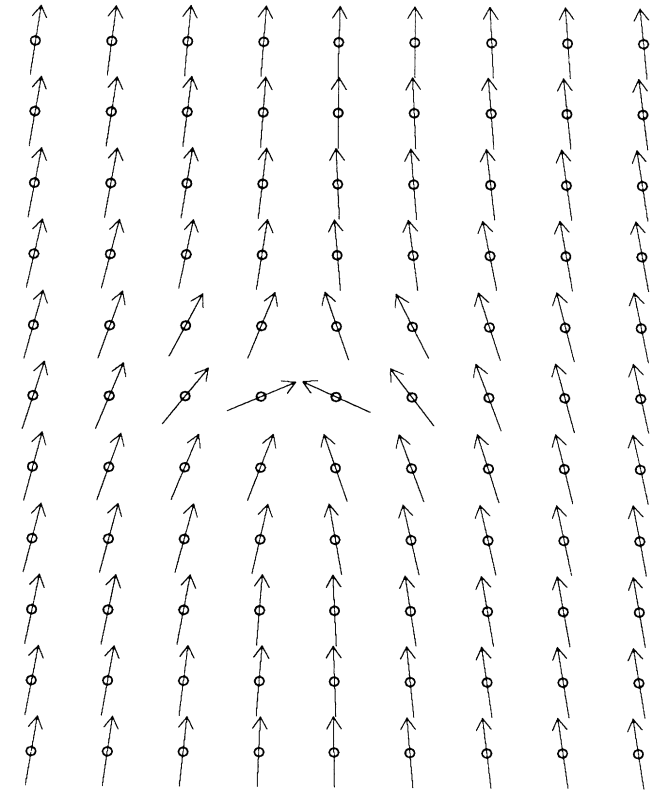


FIG. 10. Fluctuation mode for the $q_v = +\frac{1}{2}$ state of $f = \frac{1}{2}$, at $i_c^B \sim 0.109i_{c0}$.

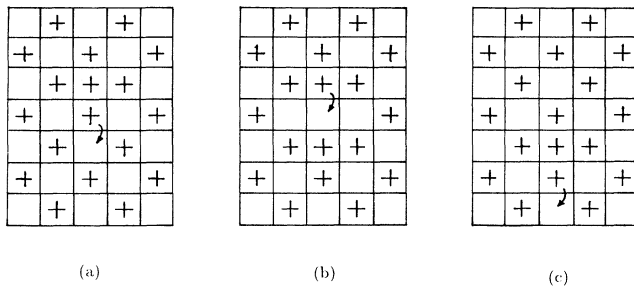


FIG. 11. Current-induced vortex motion for a $f = \frac{1}{2}$ single-extra-vortex state. The + signs represent a vorticity of +1 (or a charge of $+\frac{1}{2}$), while the open squares have zero vorticity (or a charge of $-\frac{1}{2}$). The arrows represent the movement of a unit vorticity.

of Fig. 11(b). The energy-current relation for this configuration is plotted in Fig. 12. Comparison with Fig. 7 shows that this type of excitation has much lower energies than the previous $q_v = +\frac{3}{2}$ states. The highest current that can be reached for this vortex configuration is $0.0292i_{c0}$. A stability analysis again shows that the first negative eigenvalue occurs precisely at this current. A study of the fluctuation mode responsible for this instability indicates that it corresponds to the motion of the “extra vortex” downward by one plaquette, thus replacing the displaced vortex of the checkerboard superlattice [Fig. 11(b)]. The low value of $0.029i_{c0}$ means that at the current $0.109i_{c0}$, when the first vortex motion [Fig. 11(a)] takes place, the resulting configuration [Fig. 11(b)] is already unstable to the motion of the second vortex. The combined effect of the two vortex motions is that the new configuration reached [Fig. 11(c)] is just equivalent to the original one, but shifted downward by two lattice constants. The two-step process of vortex motion is thus repeated, so that effectively an “extra” vortex moves down-

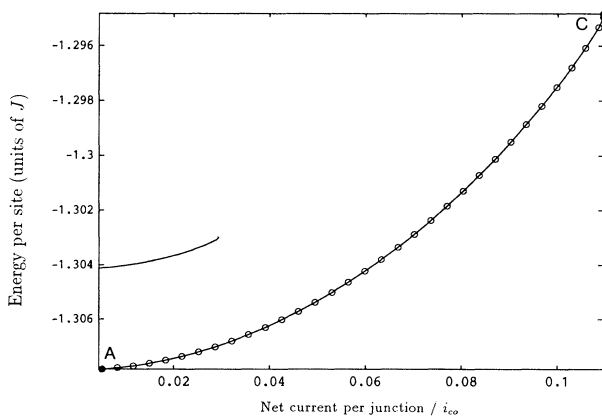


FIG. 12. Energy-current relation for $f = \frac{1}{2}$ single-extra-vortex states on a 11×9 lattice. The circled curve, equivalent to the one in Fig. 7, corresponds to the vorticity configuration of Fig. 11(a). The plain curve corresponds to the configuration in Fig. 11(b).

ward, transverse to the transport current. This is our picture of the resistive state.

A final remark is that while the linear stability analysis should be valid only for small phase deviations, it is shown that phase slips generally occur at fluctuation amplitudes of the order of unity. Therefore, although the instability due to the appropriate fluctuation modes is indisputable, their interpretation as presented above depends on the assumption that at large amplitudes these fluctuations still lead to a reduction in energy compared to the unfluctuated state.

VI. CONCLUSION

We have investigated current-induced vortex depinning in a planar Josephson-junction array. The loop current variables introduced here are a useful means of solving for stationary states. Although the detailed dynamics of phase evolution cannot be obtained from the present static model, it has been shown that a study of the fluctuation modes provides a way of interpreting instabilities in terms of the movement of vortices.

Our results show that the way in which current-induced vortex motion occurs is different for $f=0$ and $\frac{1}{2}$. While for the zero-field case the picture of a single vortex moving over a sinusoidal pinning potential is a good description, in the $f = \frac{1}{2}$ case the ground-state vortex superlattice is found to play an important role. In this latter case, vortex motion is a two-step process which involves a distortion of the checkerboard background. This means that the effective energy barrier preventing vortex motion is much lower than previously assumed, in agreement with experimental results. In this respect the analyses presented here may also be applied to other values of the magnetic field. This will reveal whether the distortion of the ground-state vortex superlattice is a general feature at finite fields. It is expected that such distortions are most likely to occur when the “vortex density” is high (with f close to $\frac{1}{2}$), so that the interaction between the extra vortex and superlattice becomes important.

While we have only considered single vortices, the analyses employed may be usefully extended to study the behavior of more complex excitations or defects. Examples of these include domain walls and multiple point defects such as vortex-antivortex pairs. Furthermore, it is of interest to examine the effect of lattice defects on vortex pinning. Cohn *et al.*²⁰ have studied such defects, which include missing junctions or even superconducting grains, from an otherwise regular array. It was found that these defects act as extrinsic pinning sites, where vortices may be “trapped.” The vortex-depinning current is generally enhanced as a result, so that vortices may be stable up to about $0.5i_{c0}$ per junction. Our analyses may contribute to an understanding of these artificially introduced pinning effects.

ACKNOWLEDGMENT

E.K.F.D. gratefully acknowledges partial financial support by the University of Bristol.

- ¹D. J. Resnick, J. C. Garland, J. T. Boyd, S. Shoemaker, and R. S. Newrock, *Phys. Rev. Lett.* **47**, 1542 (1981).
- ²Richard F. Voss and Richard A. Webb, *Phys. Rev. B* **25**, 3446 (1982).
- ³David W. Abraham, C. J. Lobb, M. Tinkham, and T. M. Klapwijk, *Phys. Rev. B* **26**, 5268 (1982).
- ⁴M. S. Rzchowski, S. P. Benz, M. Tinkham, and C. J. Lobb, *Phys. Rev. B* **42**, 2041 (1990).
- ⁵S. P. Benz, M. S. Rzchowski, M. Tinkham, and C. J. Lobb, *Phys. Rev. B* **42**, 6165 (1990).
- ⁶W. Y. Shih and D. Stroud, *Phys. Rev. B* **28**, 6575 (1983).
- ⁷S. Teitel and C. Jayaprakash, *Phys. Rev. B* **27**, 598 (1983).
- ⁸S. Teitel and C. Jayaprakash, *Phys. Rev. Lett.* **51**, 1999 (1983).
- ⁹C. J. Lobb, David W. Abraham, and M. Tinkham, *Phys. Rev. B* **27**, 150 (1983).
- ¹⁰Thomas C. Halsey, *Phys. Rev. B* **31**, 5728 (1985).
- ¹¹T. C. Halsey, *J. Phys. C* **18**, 2437 (1985).
- ¹²S. Teitel, *Physica B* **152**, 30 (1988).
- ¹³Keith A. Benedict, *J. Phys. Condens. Matter* **1**, 4895 (1991).
- ¹⁴Keith A. Benedict, *J. Phys. Condens. Matter* **3**, 5955 (1991).
- ¹⁵E. K. F. Dang, G. J. Halász, and B. L. Györfy, *Phys. Rev. B* **46**, 8353 (1992).
- ¹⁶M. Tinkham, *Physica B* **169**, 66 (1991).
- ¹⁷S. E. Korshunov and G. V. Uimin, *J. Stat. Phys.* **43**, 1 (1986).
- ¹⁸J. Villain, *J. Phys. C* **10**, 1717 (1977); **10**, 4793 (1977).
- ¹⁹W. H. Press, B. P. Flannery, S. A. Teukolsky, and W. T. Vetterling, *Numerical Recipes* (Cambridge University Press, Cambridge, England, 1988), pp. 269–272.
- ²⁰M. B. Cohn, M. S. Rzchowski, S. P. Benz, and C. J. Lobb, *Phys. Rev. B* **43**, 12 823 (1991).
- ²¹J. M. Kosterlitz and D. J. Thouless, *J. Phys. C* **6**, 1181 (1973).